

## ORBITS OF FIVE TRIPLE STARS

ANDREI TOKOVININ

Cerro Tololo Inter-American Observatory — NSF’s NOIRLab, Casilla 603, La Serena, Chile

DAVID W. LATHAM

Center for Astrophysics — Harvard & Smithsonian, 60 Garden Street, Cambridge, MA 02138, USA  
*Draft version September 23, 2020*

### ABSTRACT

Joint analysis of radial velocities and position measurements of five hierarchical stellar systems is undertaken to determine elements of their inner and outer orbits and, whenever possible, their mutual inclinations. The inner and outer periods are 12.9 and 345 yr for HD 12376 (ADS 1613), 1.14 and  $\sim 1500$  yr for HD 19971 (ADS 2390), 8.3 and 475 yr for HD 89795 (ADS 7338), 1.11 and 40 yr for HD 152027, 0.69 and 7.4 yr for HD 190412. The latter system with its co-planar and quasi-circular orbits belongs to the family of compact planetary-like hierarchies, while the orbits in HD 12376 have mutual inclination of  $131^\circ$ .

*Subject headings:* binaries:visual; binaries:general; binaries:spectroscopic

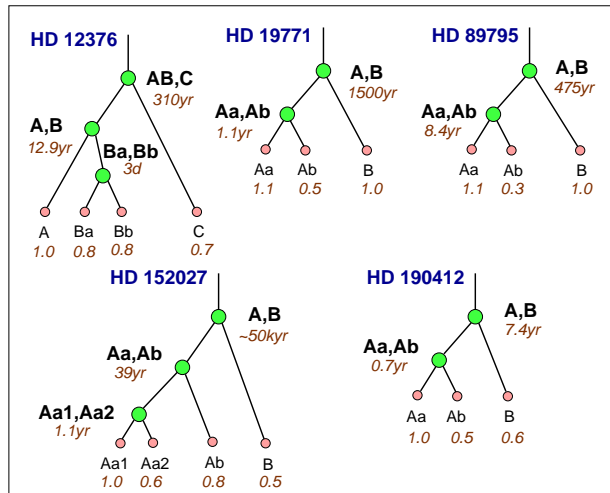


FIG. 1.— Structure of multiple systems. Green circles refer to pairs, smaller pink circles to components. Numbers in italics indicate periods and masses.

### 1. INTRODUCTION

Observational data on hierarchical stellar systems with three or more components are still incomplete and fragmentary because discovery and study of these objects is challenging. Large range of their separations and periods calls for the use of complementary techniques and/or long-term monitoring. Here we determine spectroscopic orbits of inner subsystems in five known visual binaries in the solar neighborhood. In two cases we detect astrometric signal of the inner orbit and therefore determine mutual orbit orientation. Our work contributes information on the architecture of hierarchical systems related to their origin and encoded in the mass ratios, period ratios, eccentricities, and mutual inclinations.

The five multiple systems studied here are introduced in Table 1. It gives the Washington Double Star (WDS) codes (Mason et al. 2001), HD and Hipparcos numbers,

combined visual magnitudes and parallaxes. The Gaia (Gaia collaboration 2018) parallaxes of unresolved multiple stars are notoriously unreliable, often being biased by the photo-center motion. We use unbiased parallaxes of distant single components of these systems where available or, otherwise, dynamical parallaxes derived from visual orbits and estimated masses. The last four columns of Table 1 give the types and periods of the outer and inner subsystems using codes adopted in the Multiple Star Catalog (MSC Tokovinin 2018a): V – visual orbit, A – astrometric orbit, and S1 – single-lined spectroscopic orbit. All stars are located within 67 pc from the Sun and have masses below  $1.1 M_{\odot}$ . Figure 1 illustrates the structure of these systems and their parameters. Two quadruples, HD 12376 and HD 152027, have a 3+1 hierarchy where a close inner binary has a tertiary component, and this triple is orbited by the fourth, more distant component.

The data and method of orbit calculation are presented in Section 2. Section 3 contains the results for each of the hierarchies. The paper closes with a short summary in section 4.

### 2. DATA AND METHODS

#### 2.1. Radial Velocities

Radial velocities (RVs) of these multiple systems have been monitored as part of the survey of nearby solar-type stars. The observations have been obtained at the Harvard-Smithsonian Center for Astrophysics (CfA) using several instruments on different telescopes. The Digital Speedometers (see Latham 1992) were used on 1.5 m telescopes at the Oak Ridge Observatory (Harvard, Massachusetts) and the Fred L. Whipple Observatory (Mount Hopkins, Arizona), as well as on the Multiple Mirror Telescope with an equivalent aperture of 4.5 m (also on Mount Hopkins) before its conversion to a monolithic-mirror telescope. In these instruments, intensified photon-counting Reticon detectors delivered a single echelle order  $45 \text{ \AA}$  wide centered at  $5187 \text{ \AA}$  (featuring the Mg I b triplet) at a resolving power of 35,000.

We also used the Tillinghast Reflector Echelle Spectro-

TABLE 1  
LIST OF MULTIPLE SYSTEMS

| WDS        | HD     | HIP   | $V$<br>(mag) | $\varpi$<br>(mas) | Outer | $P_{\text{out}}$<br>(yr) | Inner | $P_{\text{in}}$<br>(yr) |
|------------|--------|-------|--------------|-------------------|-------|--------------------------|-------|-------------------------|
| 02022+3643 | 12376  | 9500  | 8.14         | 19.9:             | V     | 345                      | V,S1  | 12.9                    |
| 03122+3713 | 19771  | 14886 | 7.88         | 20.58             | V     | 1500:                    | S1    | 1.14                    |
| 10217-0946 | 89795  | 50747 | 8.01         | 15.88             | V     | 475                      | A,S1  | 8.39                    |
| 16446+7145 | 152027 | 81961 | 8.66         | 14.85             | V,S1  | 39.7                     | S1    | 1.11                    |
| 20048+0109 | 190412 | 98878 | 7.69         | 20.6:             | V,S1  | 7.4                      | S1,A  | 0.69                    |

NOTE. — Explanation of columns: (1) WDS code (Mason et al. 2001); (2) HD number; (3) Hipparcos number; (4) visual magnitude; (5) parallax (colons mark less certain parallaxes); (6) type of outer orbit; (7) outer period; (8) type of inner orbit; (9) inner period.

graph (TRES; Szentgyorgyi & Fűrész 2007; Fűrész 2008) attached to the 1.5 m telescope on Mount Hopkins, which covers the wavelength range 3900–9100 Å in 51 orders at a resolving power of 44,000.

RVs were measured by cross-correlation using suitable synthetic or observed templates centered on the Mg I b triplet. The Cfa RVs are given on the native instrument system (a correction of  $+0.14 \text{ km s}^{-1}$  would be needed to bring them to the IAU system). The RVs measured with TRES have been corrected to the same zero point as the velocities from the Cfa Digital Speedometers, so they also need to be corrected by  $+0.14 \text{ km s}^{-1}$  to put them on the IAU system.

The orbits of HD 12376 and HD 89795 also use RVs measured with the CORAVEL instruments located at the Haute Provence and La Silla observatories, respectively. These observations were obtained in the framework of the large survey of solar-type stars conducted in collaboration with the Cfa team by Nordström et al. (2004); section 3.2.1 of their paper contains references on CORAVELs.

The measured RVs refer to the brightest star dominating the combined (blended) spectra of multiple systems. Blending with other components may reduce the amplitude of the RV variation. This bias is taken into consideration in the analysis of individual systems.

### 2.2. Position Measurements

All objects except the interferometric pair HD 190412 are classical visual binaries. Their orbits are based, to a large extent, on the micrometer measurements made by various observers during two centuries. These data were obtained from the WDS database (Mason et al. 2001) on our request. Obsolete discoverer’s codes are used in the WDS to identify double stars, e.g. the pairs A 1813 and BU 25 discovered by R. Aitken and S. Burnham, respectively. We follow the WDS scheme and designate components by one or several characters; systems are denoted by joining their components with a comma. For example, in a visual binary A,B the inner subsystem in component A is designated as Aa,Ab. This scheme and its extension to code the hierarchy is further explained in Tokovinin (2018a).

The subjective nature of visual measurements and different qualification of observers do not allow consistent estimates of the measurement errors. Some measurements, even those made by well-recognized observers, turn out to be erroneous or misleading when confronted with the full data set. In fitting the orbits, strong outliers are rejected, and the remaining visual measurements

are assigned errors from 50 to 250 mas, based on their scatter.

Much more accurate speckle-interferometric measurements became available starting from the late 1970s. Typical errors of early measurements on the 4 m class telescopes are about 5 mas. Measurements made with smaller telescopes have correspondingly larger errors. Modern speckle interferometers based on solid-state detectors reach an even higher accuracy of 1–2 mas (e.g. Tokovinin et al. 2019). Relative positions of binaries have been measured by Hipparcos with a typical accuracy of 10 mas; Gaia also measured component’s positions in some pairs wider than  $0''.7$ .

### 2.3. Orbit Calculation

The orbital elements derived here and their formal errors are listed in Table 2, in common notation. The ascending node  $\omega$  refers to the main component to match the RVs, and the longitude of periastron  $\Omega$  is chosen accordingly to describe the motion of the secondary, in agreement with the convention for visual orbits. In this way, both positional measurements and RVs correspond to the common set of elements. When no RV information is available, both  $\omega$  and  $\Omega$  can be simultaneously changed by  $180^\circ$  because the choice of correct orbit node remains ambiguous. Consequently, the mutual inclination  $\Phi$  can take two alternative values.

The method of orbit calculation is described in our previous paper (Tokovinin & Latham 2017).<sup>1</sup> We fit simultaneously elements of the inner and outer orbits to the data – positional measurements and RVs. Only one inner subsystem (in HD 12376) is resolved. However, in two other systems (HD 89795 and 190412) we could detect the wobble in the motion of the outer binary caused by the subsystems and determine their astrometric orbits. The wobble factor  $f$  is the ratio of the astrometric and full semimajor axes. It depends on the mass ratio  $q$  and light ratio  $r$  in the subsystem:  $f = q/(1+q) - r/(1+r)$ . When relative positions refer to the resolved inner pair or when the inner companion is faint ( $r \ll 1$ ), the second term is irrelevant and  $f$  becomes directly related to  $q$ . The inner semimajor axis of subsystems that are not directly resolved is calculated from the period and the estimated mass sum by Kepler’s Third law.

In fitting the orbits, weights inversely proportional to the squares of the measurement errors are used. An orbit should have  $\chi^2/N \sim 1$  when residuals match the errors. As noted above, the errors of positional measurements

<sup>1</sup> Codebase: <http://dx.doi.org/10.5281/zenodo.321854>

TABLE 2  
ORBITAL ELEMENTS

| WDS/system<br>Name | $P$<br>(yr)   | $T$<br>(yr) | $e$         | $a$<br>( $''$ ) | $\Omega$<br>( $^\circ$ ) | $\omega$<br>( $^\circ$ ) | $i$<br>( $^\circ$ ) | $f$         | $K_1$<br>( $\text{km s}^{-1}$ ) | $\gamma$<br>( $\text{km s}^{-1}$ ) |
|--------------------|---------------|-------------|-------------|-----------------|--------------------------|--------------------------|---------------------|-------------|---------------------------------|------------------------------------|
| 02022+3643 AB,C    | 345           | 2254.7      | 0.533       | 1.450           | 317.3                    | 319.5                    | 138.9               | ...         | ...                             | 13.76                              |
| HD 12376           | fixed         | $\pm 1.8$   | $\pm 0.018$ | fixed           | $\pm 3.9$                | $\pm 3.3$                | $\pm 1.5$           | ...         | ...                             | $\pm 0.10$                         |
| 02022+3643 A,B     | 12.903        | 1989.090    | 0.415       | 0.1496          | 191.6                    | 113.7                    | 66.1                | 0.56        | 11.02                           | ...                                |
| HD 12376           | $\pm 0.019$   | $\pm 0.036$ | $\pm 0.008$ | $\pm 0.0017$    | $\pm 0.8$                | $\pm 1.0$                | $\pm 0.7$           | $\pm 0.03$  | $\pm 0.14$                      | ...                                |
| 03122+3713 A,B     | 1500          | 1230.7      | 0.375       | 3.70            | 109.8                    | 119.4                    | 100.4               | ...         | ...                             | ...                                |
| HD 19771           | fixed         | $\pm 300$   | $\pm 0.262$ | fixed           | $\pm 5.7$                | $\pm 39$                 | $\pm 1.8$           | ...         | ...                             | ...                                |
| 03122+3713 Aa,Ab   | 1.13545       | 2002.844    | 0.462       | ...             | ...                      | 272.1                    | ...                 | ...         | 11.10                           | -20.10                             |
| HD 19771           | $\pm 0.00006$ | $\pm 0.003$ | $\pm 0.006$ | ...             | ...                      | $\pm 1.4$                | ...                 | ...         | $\pm 0.11$                      | $\pm 0.09$                         |
| 10217-0946 A,B     | 475           | 2152.8      | 0.409       | 1.28            | 250.6                    | 262.3                    | 170.0               | ...         | 0.1                             | -2.82                              |
| HD 89795           | fixed         | $\pm 2.0$   | $\pm 0.008$ | fixed           | $\pm 16.1$               | $\pm 16.6$               | fixed               | ...         | fixed                           | $\pm 0.06$                         |
| 10217-0946 Aa,Ab   | 8.39          | 2013.85     | 0.440       | 0.0734          | 208.2                    | 139.3                    | 160                 | 0.193       | 1.235                           | ...                                |
| HD 89795           | $\pm 0.08$    | $\pm 0.14$  | $\pm 0.044$ | fixed           | $\pm 8.0$                | $\pm 9.4$                | fixed               | $\pm 0.009$ | $\pm 0.088$                     | ...                                |
| 16446+7145 Aa,Ab   | 39.72         | 1995.56     | 0.399       | 0.233           | 293.4                    | 45.2                     | 124.7               | ...         | 1.68                            | -1.53                              |
| HD 152027          | $\pm 0.78$    | $\pm 0.33$  | $\pm 0.017$ | $\pm 0.004$     | $\pm 1.3$                | $\pm 2.5$                | $\pm 1.5$           | ...         | $\pm 0.15$                      | $\pm 0.09$                         |
| 16446+7145 Aa1,Aa2 | 1.1099        | 2001.144    | 0.115       | ...             | ...                      | ...                      | 73.9                | ...         | 3.392                           | ...                                |
| HD 152027          | $\pm 0.0004$  | $\pm 0.016$ | $\pm 0.012$ | ...             | ...                      | ...                      | $\pm 5.1$           | ...         | $\pm 0.048$                     | ...                                |
| 20048+0109 A,B     | 7.446         | 2018.701    | 0.202       | 0.150           | 247.7                    | 239.3                    | 32.3                | ...         | 3.01                            | -55.34                             |
| HD 190412          | $\pm 0.025$   | $\pm 0.034$ | $\pm 0.009$ | $\pm 0.003$     | $\pm 2.8$                | $\pm 3.0$                | $\pm 2.0$           | ...         | $\pm 0.10$                      | $\pm 0.03$                         |
| 20048+0109 Aa,Ab   | 0.68822       | 1998.714    | 0.039       | 0.026           | 239.5                    | 267.1                    | 31                  | 0.35        | 6.167                           | ...                                |
| HD 190412          | $\pm 0.00011$ | $\pm 0.030$ | $\pm 0.009$ | fixed           | $\pm 9.6$                | $\pm 15.8$               | fixed               | $\pm 0.07$  | $\pm 0.11$                      | ...                                |

are not known in advance; they are assigned based on the measurement technique and, if necessary, adjusted to reduce the impact of outliers. In contrast, the RV errors are known. The condition  $\chi^2/N \sim 1$  should be satisfied for both RVs and position measurements to balance their relative influence on the solution.

Long periods of some outer orbits exceed the time span of observations. Short observed arcs do not fully constrain these orbits and, instead, match a family of different orbits. For such long-period pairs, we provide a representative member of this family by fixing some elements and fitting the remaining elements. In doing so, we match the poorly constrained orbit to the expected mass sum. These notional outer orbits are needed here as a reference to measure wobble. They also constrain, to some extent, the mutual inclination. Exploration of all potential long-period orbits compatible with the observed arcs is not deemed to be necessary here.

The RVs used in spectroscopic and combined orbits and their residuals are listed in Table 4, published in full electronically. Its first two columns contain the HD number and the component to which the RV refers, followed by the Julian date, RV, its error, and residual to the orbit. The last column indicates the instrument. Individual positional measurements and their residuals from the orbits are listed in Table 5, also published electronically. Its second column indicates the pair (note that for HD 12376, A,C refers to measurements that resolve the inner pair and AB,C to the unresolved measurements between photo-center of AB and C). Then follow the data, position angle, separation, adopted error, and residuals in angle and separation. The last column specifies the techniques used. For the sake of completeness, elements of visual orbits found in the literature are reproduced in Table 3.

#### 2.4. Gaia Astrometry and Photometry

The 5-parameter astrometric solutions in the second Gaia data release (Gaia collaboration 2018) do not account for non-linear motion of the photo-center. This affects the measured parallaxes and proper motions (PMs)

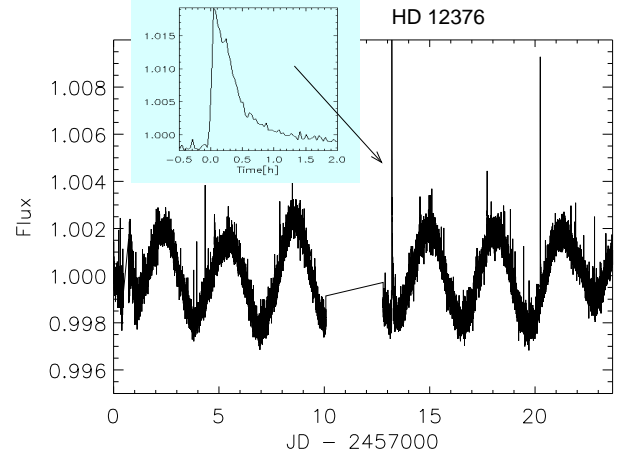


FIG. 2.— Flux modulation of HD 12376 by starspots and flares as recorded by TESS. The insert shows one flare plotted on a different time scale.

of unresolved binaries. Unusually large errors of the Gaia astrometry help to distinguish such cases, but the actual bias can exceed even these inflated errors. For this reason the Gaia PMs of unresolved binaries may not accurately reflect the PM of their photo-centers.

The  $V$  magnitudes of individual components resolved by Gaia are calculated from the  $G$  magnitudes and the BP-GP colors using the prescription given on its web site.<sup>2</sup> Effective temperatures provided by Gaia help to constrain spectral types of components. Masses in Table 6 are estimated from the absolute visual magnitudes using the standard relations of Pecaut & Mamajek (2013) for main-sequence stars. Masses of spectroscopic secondary components are estimated from their RV amplitudes or wobble, as explained below for each system.

### 3. INDIVIDUAL SYSTEMS

#### 3.1. 02022+3643 (HD 12376)

<sup>2</sup> See Chapter 5.3.7 of Gaia DR2 documentation at <https://gea.esac.esa.int/archive/documentation/GDR2/>.

TABLE 3  
PREVIOUSLY PUBLISHED ORBITAL ELEMENTS

| WDS/system       | $P$<br>(yr) | $T$<br>(yr) | $e$   | $a$<br>( $''$ ) | $\Omega$<br>( $^\circ$ ) | $\omega$<br>( $^\circ$ ) | $i$<br>( $^\circ$ ) | Reference                    |
|------------------|-------------|-------------|-------|-----------------|--------------------------|--------------------------|---------------------|------------------------------|
| 02022+3643 AB,C  | 310         | 2210.24     | 0.636 | 1.790           | 168.5                    | 135.5                    | 113.2               | Novakovic & Todorovic (2006) |
| 02022+3643 A,B   | 12.94       | 1989.06     | 0.404 | 0.15            | 191.4                    | 295.1                    | 67.0                | Hartkopf et al. (2000)       |
| 03122+3713 A,B   | 871         | 1454        | 0.710 | 3.66            | 111.0                    | 105.0                    | 98.0                | Mason et al. (2004)          |
| 10217-0946 A,B   | 817         | 2295        | 0.0   | 1.837           | 0.2                      | 0.0                      | 141.2               | Zirm & Rica (2012)           |
| 16446+7145 Aa,Ab | 62.0        | 1977.5      | 0.19  | 0.263           | 64.7                     | 358.0                    | 121.0               | Heintz (1997)                |
| 20048+0109 A,B   | 7.83        | 2018.61     | 0.256 | 0.164           | 74.3                     | 47.6                     | 40.5                | Tokovinin (2018b)            |

TABLE 4  
RADIAL VELOCITIES AND RESIDUALS (FRAGMENT)

| HD    | Comp. | JD<br>(JD -24,00,000) | RV      | $\sigma$<br>( $\text{km s}^{-1}$ ) | (O-C)  | Instr. <sup>a</sup> |
|-------|-------|-----------------------|---------|------------------------------------|--------|---------------------|
| 12376 | A     | 43519.2870            | 2.830   | 1.000                              | 0.110  | COR                 |
| 12376 | A     | 43519.2910            | 4.160   | 1.000                              | 1.440  | COR                 |
| 19771 | Aa    | 49558.9932            | -26.610 | 0.490                              | -0.131 | CfA                 |

<sup>a</sup> Instruments: CfA: CfA digital speedometers; MMT: CfA speedometer on MMT; TRES: TRES; COR: CORAVEL; TS2002: Tokovinin & Smekhov (2002); Butler: Butler et al. (2017) with a  $-55.04 \text{ km s}^{-1}$  offset.

TABLE 5  
POSITION MEASUREMENTS AND RESIDUALS (FRAGMENT)

| HD    | Syst. | Date<br>(JY) | $\theta$<br>( $^\circ$ ) | $\rho$<br>( $''$ ) | $\sigma_\rho$<br>( $''$ ) | (O-C) $_\theta$<br>( $^\circ$ ) | (O-C) $_\rho$<br>( $''$ ) | Ref. <sup>a</sup> |
|-------|-------|--------------|--------------------------|--------------------|---------------------------|---------------------------------|---------------------------|-------------------|
| 12376 | A,B   | 1908.8100    | 188.5                    | 0.2000             | 0.0500                    | 2.2                             | 0.0396                    | M                 |
| 12376 | A,B   | 1918.6600    | 163.0                    | 0.2100             | 0.1000                    | 6.1                             | 0.0800                    | M                 |
| 12376 | A,C   | 1999.8843    | 207.6                    | 1.4940             | 0.0050                    | -0.2                            | -0.0025                   | s                 |
| 12376 | A,C   | 2010.7185    | 200.0                    | 1.6063             | 0.0050                    | -0.1                            | -0.0002                   | s                 |
| 12376 | AB,C  | 1991.2500    | 216.0                    | 1.4210             | 0.0200                    | 1.1                             | 0.1030                    | H                 |
| 12376 | AB,C  | 2015.5000    | 199.2                    | 1.5520             | 0.0050                    | 0.2                             | -0.0031                   | G                 |

<sup>a</sup> C: CCD measurement; G: Gaia; H: Hipparcos; M: visual micrometer measurement; P: photographic measurement; S: speckle interferometry at SOAR; s: speckle interferometry at other telescopes.

TABLE 6  
VISUAL MAGNITUDES AND MASSES

| HD     | Component | $V$<br>(mag) | Mass<br>( $M_\odot$ ) |
|--------|-----------|--------------|-----------------------|
| 12376  | A         | 8.80         | 0.95                  |
|        | B         | 9.00         | 1.62                  |
|        | C         | 10.79        | 0.72                  |
| 19771  | Aa        | 7.88         | 1.08                  |
|        | Ab        | ...          | 0.47                  |
|        | B         | 8.16         | 1.03                  |
| 89795  | Aa        | 8.44         | 1.07                  |
|        | Ab        | ...          | 0.27                  |
|        | B         | 9.12         | 0.96                  |
| 152027 | Aa1       | 9.15         | 0.98                  |
|        | Aa2       | ...          | 0.6                   |
|        | Ab        | 10.21        | 0.83                  |
|        | B         | 13.88        | 0.54                  |
| 190412 | Aa        | 7.75         | 0.97                  |
|        | Ab        | ...          | 0.45                  |
|        | B         | 11.37        | 0.61                  |

This is a quadruple system of 3+1 hierarchy, also known as ADS 1613. The visual triple A 1813 A,B and AB,C has been discovered by R. Aitken in 1908. Both inner and outer systems have known visual orbits, refined here. Moreover, the inner secondary component B is a double-lined spectroscopic pair with  $P = 3.082 \text{ d}$  (M.

Mayor, 1995, private communication). Precise photometry by the Transiting Exoplanet Survey Satellite (TESS, Ricker et al. 2014) shows flux modulation with a period of 3.1 d, presumably caused by starspots on tidally locked stars Ba and Bb, and flares in their active chromospheres (Figure 2).<sup>3</sup> The close binary Ba,Bb is not eclipsing. The Gaia parallax of  $19.44 \pm 0.17 \text{ mas}$  may be biased, and we adopt instead the dynamical parallax of 19.9 mas deduced from the well-defined inner orbit and the estimated mass sum.

The RVs refer to the blended light of A and B (the contribution of C, at  $1''.5$  from AB and 2.7 mag fainter, can be neglected). Only the lines of the brightest star A are measured. Broad lines produced by Ba and Bb are detectable in the cross-correlation function, but no RVs were extracted so far.

The inner combined visual/spectroscopic orbit with  $P = 12.9 \text{ yr}$  is very well constrained by the century-long astrometry and the RVs (Figure 3). The RV residuals of  $1 \text{ km s}^{-1}$  exceed the internal RV errors, possibly because of blending with the lines of Ba and Bb. We adopted RV

<sup>3</sup> A photometric period of  $1^{\text{d}}.4937$  was previously determined for this star designated as V371 And. This can be an alias of the 3 day period.

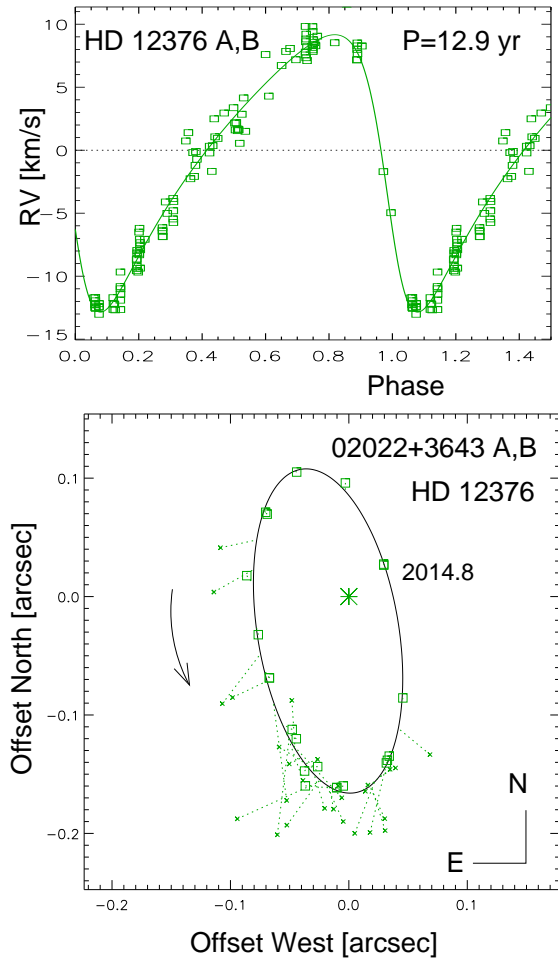


FIG. 3.— Orbit of HD 12376 A,B with  $P = 12.9$  yr. The upper panel plots RVs vs. orbital phase, the lower panel plots the position measurements (squares for speckle data, crosses for less accurate micrometer data). Dotted lines connect the measured positions to the ephemeris positions on the orbit (ellipse).

errors of  $1 \text{ km s}^{-1}$  and discarded two most discrepant measurements. The weighted residuals of speckle positions are 6 mas. The orbital inclination, the estimated mass of A,  $0.95 M_{\odot}$ , and its RV amplitude correspond to the mass of  $1.62 M_{\odot}$  for B. This matches the standard relations if B is composed of two equal stars of  $V = 9.75$  mag each. The mass sum of AB,  $2.57 M_{\odot}$ , corresponds to the dynamical parallax of 19.9 mas.

Incomplete coverage of the outer orbit (Figure 4) leaves its elements less well defined. After the initial free fit, we fixed the outer period and semimajor axis to match the expected mass sum of  $3.3 M_{\odot}$  and the dynamical parallax deduced from the inner orbit. Most available measurements refer to the unresolved outer pair AB,C, but two resolved measurements of A,C were published by Horch et al. (2017). They allow us to determine the wobble factor  $f = 0.56 \pm 0.03$ . Obviously, B is more massive than A; our estimated masses imply  $f = 0.63$ .

The outer orbit corresponds to the RV amplitude of  $1.5 \text{ km s}^{-1}$  for AB and predicts a negative RV trend tentatively seen in the residuals. However, the 18-yr RV coverage (1978–1996) is not long enough to measure the outer RV amplitude. The choice of the outer nodes remains ambiguous. It corresponds to the mutual orbit inclination of  $\Phi = 131 \pm 3^{\circ}$ . The inner and outer pairs of

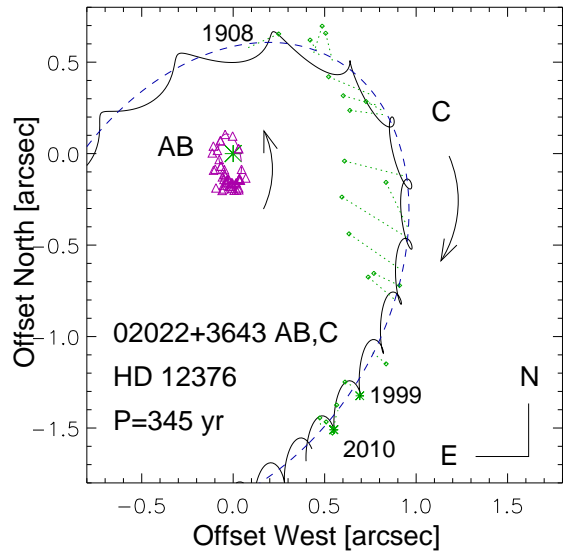


FIG. 4.— Fragment of the orbit of HD 12376 AB,C with  $P = 345$  yr. Solid line and asterisks depict the motion of A,C (i.e. the resolved inner system), while dashed line and crosses refer to the unresolved orbit of AB,C. The inner orbit of A,B is shown for reference on the same scale by the magenta ellipses and triangles. Note opposite rotation sense of the inner and outer orbits.

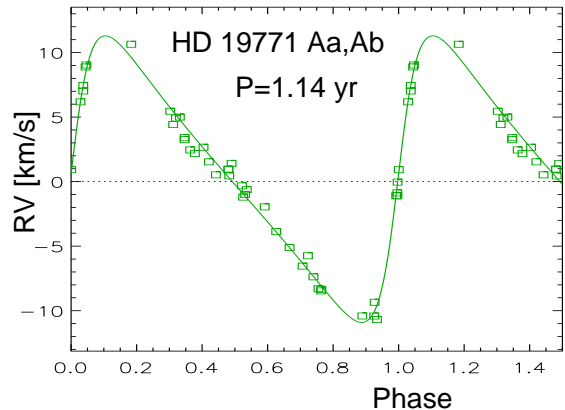


FIG. 5.— Spectroscopic orbit of HD 19771 Aa,Ab.

ADS 1613 rotate in opposite sense (Figure 4). Alternative choice of the outer node corresponds to orthogonal orbits ( $\Phi = 87^{\circ}$ ), which would produce a strong modulation of inner eccentricity and therefore seems unlikely.

### 3.2. 03122+3713 (HD 19771)

The outer pair is a classical visual binary STF 360 (ADS 2390) discovered by W. Struve in 1828 at  $1''.2$  separation. It slowly opened up and is now at  $2''.9$ . Only a small arc of the outer orbit is covered and its long period remains poorly constrained; a preliminary orbit with  $P = 871$  yr was published by Mason et al. (2004). RV variability of the brighter star A was detected by Nordström et al. (2004); its orbit with a period of 1.14 yr is determined here. Motion of the photo-center caused by the one-year subsystem seriously biases the Gaia parallax,  $24.42 \pm 0.66$  mas. The more reliable parallax of star B,  $20.58 \pm 0.09$  mas, is adopted here as distance to the system.

There was a suspicion that RV of B is also variable with a small amplitude. However, close proximity of the two stars might cause partial mixing of their light in the

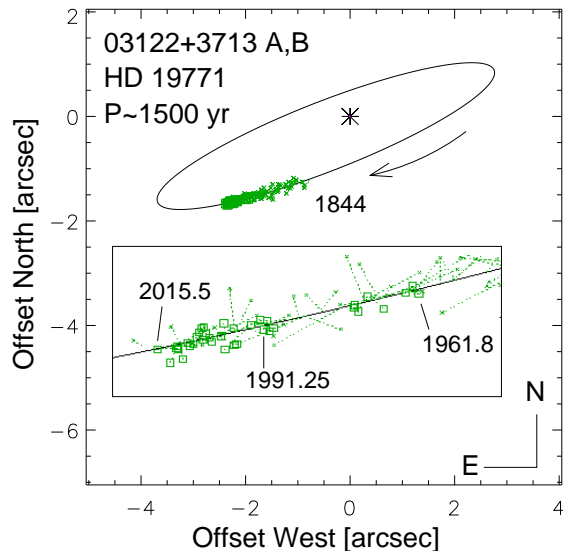


FIG. 6.— Tentative visual orbit of WDS 13122+3713 A,B (HD 19771). Squares show positions with errors of less than 60 mas, crosses are less accurate micrometer measurements. The insert shows the latest data in detail.

slit, hence the RV variability of B remains questionable. Tokovinin & Smekhov (2002) published 30 RVs of A and 23 RVs of B monitored with a CORAVEL-type correlation instrument during six years. Their data do not confirm the RV variability of B.

The spectroscopic orbit of Aa,Ab is well defined (Figure 5). We fitted the orbit separately to 16 RVs from CfA covering the period 1994–2014 or 27 RVs from Tokovinin & Smekhov (2002) measured in 1992–1998. Both data sets show excessive noise, while the systemic velocities agree within  $0.1 \text{ km s}^{-1}$ . The final orbit uses all data (the errors of RVs from Tokovinin & Smekhov 2002, are set to  $0.6 \text{ km s}^{-1}$ ) and leaves the weighted rms residuals of  $0.43 \text{ km s}^{-1}$ . The orbit of Aa,Ab corresponds to the minimum mass of  $0.47 M_{\odot}$  for Ab. The mass can be larger, but not by too much, otherwise the lines of Ab would be detectable in the spectrum.

A plausible but otherwise arbitrary orbit of the outer visual pair A,B with  $P = 1500 \text{ yr}$  is illustrated in Figure 6. Its period and semimajor axis are chosen to match the expected mass sum of  $2.58 M_{\odot}$ . Owing to the wide separation, there are no speckle measurements. Instead, the most accurate astrometry is furnished by the photographic and CCD measurements, as well as by Gaia and Hipparcos.

Residuals to the orbit of A,B were analyzed to search for a potential wobble signal. No obvious periodicity was found. If only accurate data (errors less than 60 mas) are considered and the residuals exceeding  $0''.1$  are ignored, the rms scatter of the remaining residuals is 21 mas in separation and  $0''.25$  in angle (12 mas in tangential direction). It is well known that separations are measured less accurately than angles because of the partial image blurring, so larger residuals in separation are natural. A tentative orbit of Ba,Bb deduced from the CfA RVs has a period of 15.4 yr, semi-amplitude  $1.75 \text{ km s}^{-1}$ , and implies a Ba,Bb semimajor axis of  $0''.13$ . The RVs from Tokovinin & Smekhov (2002) do not match this orbit, however. Absence of wobble larger than  $\sim 20 \text{ mas}$  constrains parameters of a potential subsystem in the

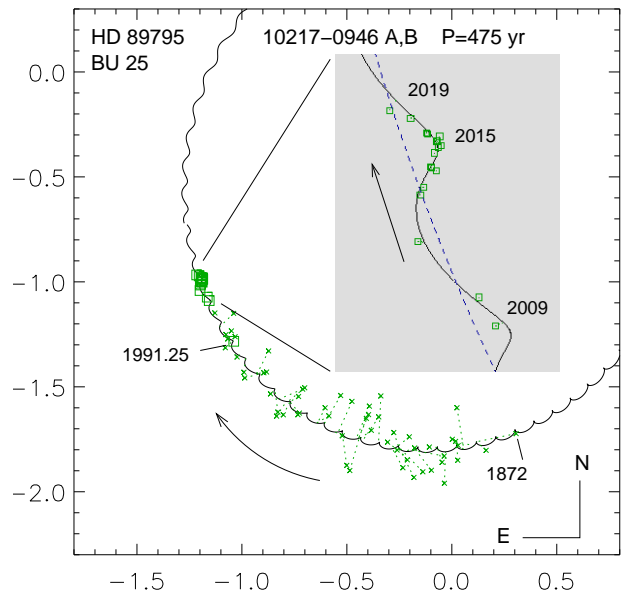


FIG. 7.— Orbital motion of HD 89795 (WDS J10217-0946, BU 25) A,B. Observed part of the orbit (including wobble) is plotted by the full line. The micrometer and low-accuracy speckle measurements are plotted by crosses, the accurate speckle and Hipparcos measurements by squares. The insert shows the orbit segment covered at SOAR.

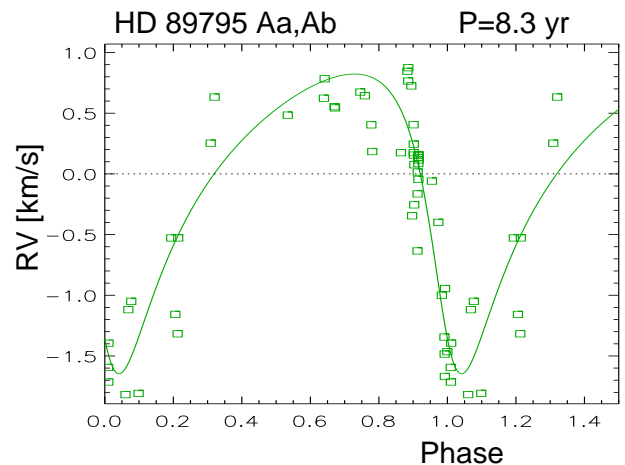


FIG. 8.— Spectroscopic orbit of the inner 8.3 yr subsystem HD 89795 Aa,Ab.

component B. Its existence cannot be ruled out but, so far, remains unproven.

The calculated amplitude of the wobble caused by the subsystem Aa,Ab is about 8 mas. Such a weak signal is not detectable at the current accuracy of A,B measurements but biases the Gaia parallax, as noted above. Hopefully, future Gaia data releases will separate orbital and parallactic motions of A and will define its astrometric orbit. The PM of B relative to A measured by Gaia is  $(+3.0, +6.5) \text{ mas yr}^{-1}$ . The relative motion speed in the outer orbit is  $(+8.5, -2.0) \text{ mas yr}^{-1}$ . The discrepancy is presumably caused by the motion of Aa,Ab and matches the PM anomaly (Brandt 2018).

### 3.3. 10217-0946 (HD 89795)

The outer pair of HD 89795 (WDS J10217-0946, BU 25, ADS 7738) was discovered by S. W. Burnham

in 1872 at  $1''.75$  separation. Since then, it has turned clockwise by  $61^\circ$ . Gaia parallaxes are  $16.25 \pm 0.11$  mas for A and  $15.88 \pm 0.08$  mas for B. The latter, unbiased by the inner subsystem, is adopted as true distance.

A spectroscopic subsystem in the component A was found by Nordström et al. (2004). They observed this star using CORAVEL from 1988.2 to 1997.2. Follow-up observations were conducted with the CfA digital spectrometer from 2004.0 to 2009.3 and the last RV was measured with TRES in 2014.1. The RV data cover 25.2 yr or 3.1 inner periods. The RVs of the visual secondary star B were also measured at CfA 15 times. Their mean value is  $-3.28$  km s $^{-1}$  with the rms scatter of  $0.69$  km s $^{-1}$  around the mean (un-weighted).

The preliminary spectroscopic orbit of Aa,Ab with a period of 3056 days (8.37 yr) computed by D. W. L. in 2009 implied an inner semimajor axis of 76 mas. Therefore, a wobble in the observed motion of the outer pair A,B was expected. This pair has been placed on the speckle interferometry program at the 4.1 m Southern Astrophysical Research (SOAR) telescope and monitored for ten years, from 2009.26 to 2019.95 (Tokovinin et al. 2019, and references therein). The spectroscopic subsystem has not been resolved, but accurate measurements enabled detection of the expected wobble.

A preliminary orbit of A,B with  $P = 817$  yr was computed by Zirm & Rica (2012), assuming zero eccentricity. The short observed arc does not constrain the outer orbit well enough. Here elements of the outer and inner orbits are fitted jointly to determine the inner astrometric orbit. As no resolved measurements of the inner subsystem are available, its semimajor axis was fixed at the calculated value of 73.4 mas. The resulting wobble factor  $f = 0.193 \pm 0.009$  is measured reliably and corresponds to the wobble amplitude  $\alpha = 14.2 \pm 0.7$  mas.

Finding an optimum set of orbital elements describing all data was not trivial because both inner and outer orbits have small inclinations, i.e. are oriented almost in the plane of the sky. This follows from the small RV amplitude of the inner orbit and from the near-coincidence of the mean RVs of A and B; their difference is much less than a few km s $^{-1}$  implied by our first-guess outer circular orbit. In the final iteration, we fixed the outer inclination to  $175^\circ$  to obtain a small but non-zero RV difference between A and B. The final values of  $P$  and  $a$  were also fixed to match the mass sum of  $2.33 M_\odot$ . The RV difference between A and B is so small that even its sign (which defines the correct node of the outer orbit) is not established reliably. No RV trend due to the outer orbit is detectable. So, we simply fixed the outer RV amplitudes to 0.1 and 0.15 km s $^{-1}$ . These amplitudes have only a minor effect on the center-of-mass velocity.

The orbital solution including wobble results in the rms RV residuals of  $0.37$  km s $^{-1}$ , matching the RV errors ( $\chi^2/N \approx 1$ ). The weighted rms astrometric residuals are 3 mas. They are comparable to the residuals of the calibration binaries observed at SOAR to their modeled motion (Tokovinin et al. 2019). The Gaia measurement of A,B was not used to avoid a small difference in the scale noted before (it fits the orbit well if the separation is increased by 9 mas). Residuals to the orbit fitted with zero wobble increase to 14 mas. Figure 7 shows the observed arc of the A,B orbit and the zoom on the SOAR data. Figure 8 gives the RV curve of the inner orbit with

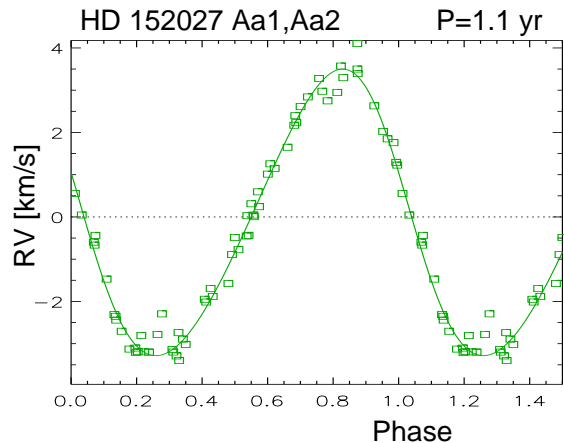


FIG. 9.— Spectroscopic orbit of HD 152027 Aa1,Aa2.

the outer orbit subtracted. The elements of both orbits and their errors are given in Table 2. The preliminary spectroscopic orbit of Aa,Ab by D. W. L. had  $K_1 = 1.23$  km s $^{-1}$ ,  $\gamma = -2.90$  km s $^{-1}$ ,  $e = 0.50$ ,  $\omega = 140^\circ.6$ . Owing to the small RV amplitude caused by face-on orbit orientation, positional measurements have a substantial influence on the combined inner orbit.

The masses of stars Aa and B estimated from their absolute  $V$  magnitude using standard relations (Pecaut & Mamajek 2013) are 1.07 and 0.96  $M_\odot$ , respectively. The wobble factor  $f = 0.193$  implies the inner mass ratio  $q_{Aa,Ab} = f/(1-f) = 0.25$ , hence the mass of Ab is  $0.27 M_\odot$ . The inner RV amplitude and inclination fixed to  $i_{Aa,Ab} = 160^\circ$  match this mass. A free fit leads to  $i_{Aa,Ab} \approx 180^\circ$ , incompatible with the observed RV variation of Aa.

Both inner and outer binaries have retrograde (clockwise) motion. The adopted node of the outer orbit corresponds to the mutual inclination  $\Phi = 17 \pm 2^\circ$ ; the alternative value obtained by swapping the nodes is  $24^\circ$ . As both orbits are seen almost face-on, the two values of mutual inclination are close to each other.

Gaia measured a notable difference between the PMs of B and A,  $(-3.1, +10.5)$  mas yr $^{-1}$  in R.A. and declination, respectively. Our two orbits predict the motion of B relative to A in 2015.5 with a speed of  $(-4.2, +8.3)$  mas yr $^{-1}$ , in reasonable agreement with Gaia. Our astrometric orbit of Aa,Ab approximately matches the observed PM anomaly — the difference between the short-term PM measured by Gaia and the long-term PM deduced from Gaia and Hipparcos positions. According to Brandt (2018), it is  $(8.26, 2.06)$  mas yr $^{-1}$  in the R.A. and declination directions. The inner orbit predicts the PM anomaly of  $(-8.9, -4.7)$  mas yr $^{-1}$ . The sign is inverted because, according to the convention, visual elements describe motion of Ab around Aa while the PM anomaly refers to Aa.

### 3.4. $16446+7145$ (HD 152027)

This is a quadruple system of 3+1 hierarchy. The outer  $27''.6$  common proper motion pair UC 3219 A,B is physical. The parallax of the faint ( $V = 13.88$  mag) secondary star B,  $14.854 \pm 0.035$  mas, defines the distance to the system (Gaia does not provide astrometry for the inner triple). The intermediate subsystem is a visual binary MLR 182 Aa,Ab known since 1971. Finally, star

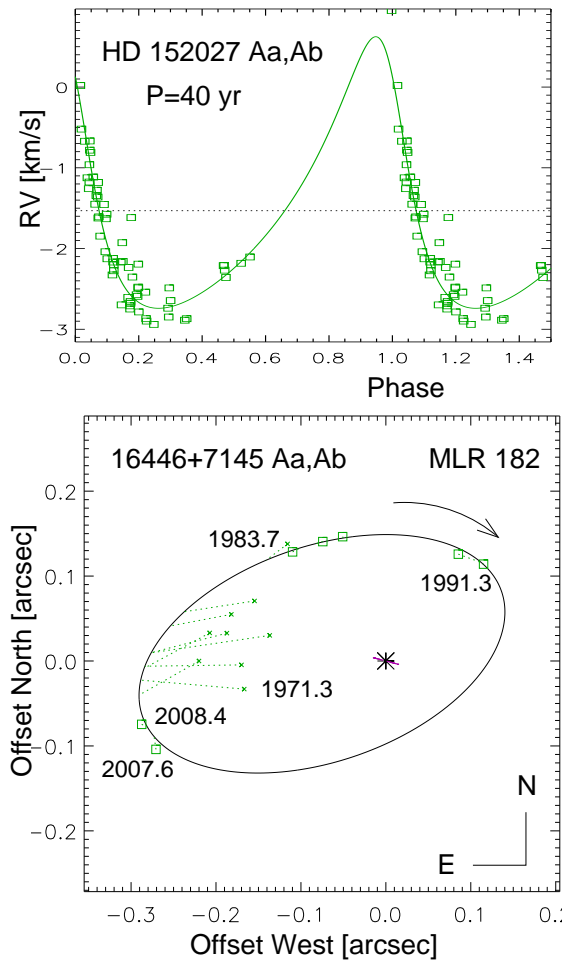


FIG. 10.— Combined orbit of HD 152027 (WDS J16446+7145, MLR 182) Aa,Ab

Aa is itself a spectroscopic binary with a period of 405 d discovered at CfA (Figure 9). It was recognized as a spectroscopic triple and a preliminary outer period of 26.5 yr was determined by D. W. L. from RVs measured during a 22 yr period, 1995–2017. Seven RVs come from TRES. The weighted rms residuals to the orbits determined here,  $0.19 \text{ km s}^{-1}$ , match the RV errors. However, we ignored the first three slightly discrepant RVs.

The tentative visual orbit of Aa,Ab with  $P = 63 \text{ yr}$  by Heintz (1997) is revised here to  $P = 40 \text{ yr}$  using both the position measurements and the RVs. The latest two speckle measurements by Mason et al. (2011), made in 2007 and 2008, at first appeared highly discrepant. B. Mason has checked them on our request and found no errors. This confirmation prompted us to re-consider the orbit and, finally, a good solution that fits both RVs and speckle data was found with the change of quadrants in 2007 and 2008 (Figure 10). One full revolution is covered. However, the new orbit deviates from the early visual measurements that systematically under-estimate the separation. The highly discrepant visual measurement by Heintz in 1996 was rejected. The new orbit gives the mass sum of  $2.44 M_{\odot}$  for A. Given the small number of accurate speckle measurements, we did not try to determine the wobble. The inner semimajor axis is  $18.5 \text{ mas}$ , the estimated wobble amplitude is  $\sim 7 \text{ mas}$ . Frequent speckle measurements during a couple of years

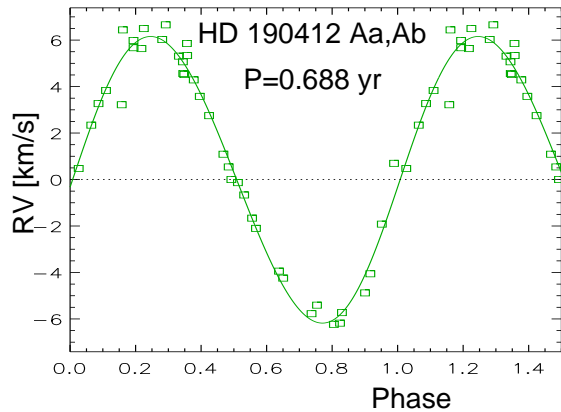


FIG. 11.— Spectroscopic orbit of HD 190412 Aa,Ab.

would easily detect the wobble, while Gaia might provide an astrometric orbit in the future.

The visual orbit together with estimated masses implies an RV amplitude of  $3 \text{ km s}^{-1}$ , whereas the measured amplitude in the outer orbit,  $1.7 \text{ km s}^{-1}$ , corresponds to an unrealistically small mass of star Ab. A likely explanation of this discrepancy is blending of lines that reduces the measured RV amplitude. The inner amplitude is likewise reduced by both blending and inclination, and we tentatively assign a mass of  $0.6 M_{\odot}$  to Aa2 to match approximately the measured mass sum of the visual pair Aa,Ab.

### 3.5. 20048+0109 (HD 190412)

This is a nearby (Gaia parallax  $29.60 \pm 0.52 \text{ mas}$ ) compact triple system. It has been identified as a single-lined spectroscopic triple with periods of 251 d and 7.8 yr in the CfA RV survey; Nordström et al. (2004) also found the RV to be variable. The outer pair produces acceleration measured by Hipparcos. It has been resolved by the speckle camera at SOAR in 2015 (TOK 699) and has been followed for 4.4 yr, covering most of the outer orbit. Speckle photometry reveals a substantial magnitude difference between A and B, 2.5 mag in  $I$  and 3.9 mag in  $V$ . A preliminary 7.8 yr visual orbit was published by Tokovinin (2018b). Joint analysis of the RVs and speckle interferometry results in the combined outer orbit presented here. Owing to the small period ratio, the orientation of the inner orbit could be determined from the wobble.

Figure 11 shows the inner spectroscopic orbit with the contribution of the outer orbit subtracted. We added five precise RVs measured by Butler et al. (2017) in 2003–2006 with an offset of  $-55.04 \text{ km s}^{-1}$  deduced from our preliminary orbits (these RVs are only relative). Their first RV deviates by  $1.5 \text{ km s}^{-1}$  and is given a low weight, as well as two CfA RVs. The remaining data are excellent, with the rms of only  $0.14 \text{ km s}^{-1}$ . Deviant RVs are likely produced by blending with other components. Figure 12 illustrates the outer orbit. Initially, the wobble amplitude was set to zero, then the inner elements  $\Omega$ ,  $i$ , and  $f$  were fitted jointly with both orbits. The inner inclination is poorly constrained by the data and was fixed to  $31^{\circ}$  to match the inner RV amplitude (a free fit converges to  $i = 0$ , contradicting the RV variability). Including wobble in the model reduces the rms residuals of speckle measurements from 6 mas to 2 mas, indicat-



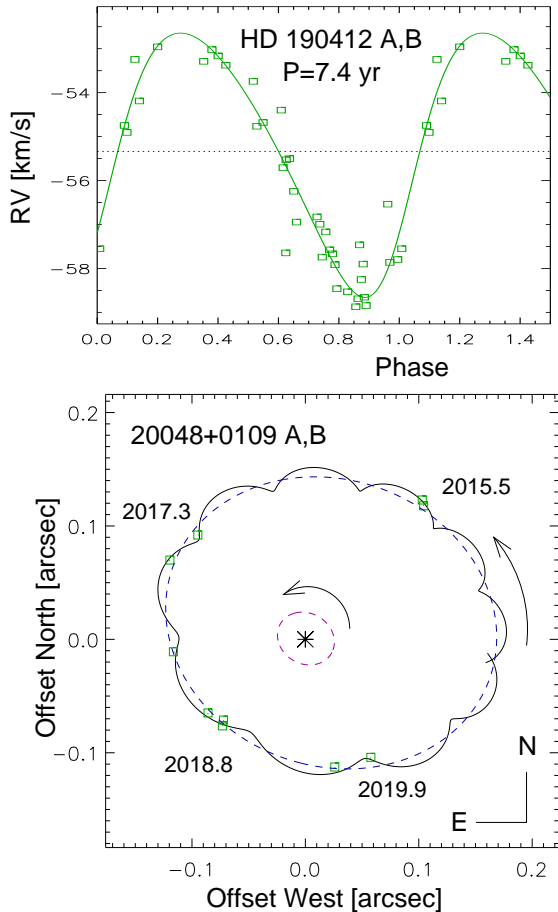


FIG. 12.— Combined outer orbit of HD 190412 (TOK 699) A,B. The full line depicts orbit with wobble, the blue dashed line shows orbit without wobble, and the small ellipse at the center shows the inner orbit.

ing that the astrometric signal is significant. The inner semimajor axis of 26 mas is computed and the wobble factor  $f = 0.35 \pm 0.07$  is found. It implies the inner mass ratio of  $0.54 \pm 0.15$ , while the RV amplitude together with the adopted inner inclination implies  $q = 0.46$ . Therefore, the masses of Aa, Ab, and B of 0.97, 0.45, and 0.61  $M_{\odot}$ , respectively, approximately match all data. The outer RV amplitude computed using those masses is  $3.32 \text{ km s}^{-1}$ , the measured amplitude is  $3.01 \text{ km s}^{-1}$ . Light of fainter stars Ab and B slightly reduces the measured RV amplitudes by blending with the spectrum of Aa.

The outer orbit is very well defined. Adopting the outer mass sum of  $2.04 M_{\odot}$ , we obtain the dynamical parallax of 31 mas, which compares well with the likely biased Gaia parallax of 29.6 mas. Fuhrmann & Chini (2019) took one high-resolution spectrum of HD 190412 in 2017.625 and detected a slight asymmetry of the lines caused by a weak component with an RV shifted by  $+11.4 \text{ km s}^{-1}$  relative to the stronger lines. They modeled the spectrum by a combination of three stars with effective temperatures of 5650, 3900, and 4100 K and solar metallicity. Our orbits predict that on this date the RV of B was shifted by  $+10.8 \text{ km s}^{-1}$  relative to Aa, in qualitative agreement with the Fuhrmann’s result.

The most remarkable property of this system is the orbit coplanarity: the mutual inclination is  $\Phi = 6 \pm 4^{\circ}$ , with a caveat that the inner inclination is not well constrained.

Note also the small eccentricities of inner and outer orbits. The period ratio is  $10.82 \pm 0.04$ . This triple system belongs to the family of “planetary-like” hierarchies like HD 91962 (Tokovinin et al. 2015), where the inner periods of 0.47 and 8.8 yr are similar to those of HD 190412 and, likewise, the orbits have moderate eccentricities and are approximately coplanar. Similar architecture is encountered in some other multiple systems with low-mass components.

#### 4. SUMMARY

Our work contributed inner spectroscopic orbits in several hierarchical systems composed of low-mass stars. In two instances (HD 89795 and 190412), accurate speckle-interferometric measurements of the outer pairs allowed us to detect wobble produced by the inner subsystems. Astrometric orbits of these subsystems are determined and mutual inclinations between inner and outer orbits are established; both systems are approximately aligned and co-rotate. In contrast, mutual inclination in the resolved triple HD 12376 is large,  $131^{\circ}$ ; the inner and outer pairs are counter-rotating. Moreover, this system contains an inner close pair Ba,Bb. Architecture of HD 12376 differs markedly from that of planar planetary-like systems, hinting that hierarchies in the solar neighborhood might be produced by different mechanisms.

This study is enabled by long-term monitoring of RVs on a time scale of decades and position measurements spanning up to two centuries. The accuracy and resolution of modern techniques, especially space experiments like Gaia, give access to a vast number of hierarchical systems, but the time coverage is and will remain a major limiting factor. Orbital periods of typical stellar and planetary systems range from years to centuries and call for a patient accumulation of data.

D. W. L. thanks the many observers, especially Robert Stefanik, Joe Caruso, Joe Zajac, Mike Calkins, Perry Perlind, and Gil Esquerdo, who obtained observations with the CfA Digital Speedometers on telescopes in Massachusetts and Arizona, and with TRES on the 1.5-m Tillinghast Reflector at the Fred L. Whipple Observatory. We thank Stephane Udry for sharing the radial velocities of HD 12376 ABC from observations obtained with the northern CORAVEL on the SWISS 1.0-m telescope at the Observatoire de Haute Provence, and the radial velocities of HD 89795 from the southern CORAVEL on the Danish 1.54-m telescope at the European Southern Observatory on La Silla.

Some data used here were obtained at the Southern Astrophysical Research (SOAR) telescope. This work used the SIMBAD service operated by Centre des Données Stellaires (Strasbourg, France), bibliographic references from the Astrophysics Data System maintained by SAO/NASA, and the Washington Double Star Catalog maintained at USNO. We thank B. Mason for extracting historic measurements from the WDS database and checking his speckle measurements of HD 152027. This paper includes data collected by the TESS mission funded by NASA’s Science Mission directorate. This work has made use of data from the European Space Agency (ESA) mission Gaia (<https://www.cosmos.esa.int/gaia>),

processed by the Gaia Data Processing and Analysis Consortium (DPAC, <https://www.cosmos.esa.int/web/gaia/dpac/consortium>). SOAR, Gaia, TESS, ADS, OHP:1.0 (CORAVEL), Danish 1.54-m Telescope (CORAVEL), FLWO:1.5m (TRES, DS), ORO:Wyeth (DS), MMT (DS) institutions, in particular the institutions participating in the Gaia Multilateral Agreement.

## REFERENCES

- Brandt, T. D. 2018, *ApJS*, 239, 31  
 Butler, R. P., Vogt, S. S., Laughlin, G., et al. 2017, *AJ*, 153, 202  
 Fűrész, G. 2008, PhD thesis, University of Szeged, Hungary  
 Fuhrmann, K. & Chini, R. 2019, *MNRAS*, 482, 471  
 Gaia Collaboration, Brown, A. G. A., Vallenari, A., Prusti, T., et al. 2018, *A&A*, 595, 2 (*Vizier Catalog I/345/gaia2*).  
 Hartkopf, W. I., Mason, B. D., McAlister, H. A., et al.,  
 Hartkopf, W. I., Mason, B. D. & Worley, C. E. 2001, *AJ*, 122, 3472  
 Heintz, W. D. 1997, *ApJS*, 111, 335  
 Horch, E. P., Casetti-Dinescu, D. I., Camarata, M. A., et al. 2017, *AJ*, 153, 212  
 Latham, D. W. 1992, in *IAU Coll. 135, Complementary Approaches to Double and Multiple Star Research*, ASP Conf. Ser. 32, eds. H. A. McAlister & W. I. Hartkopf (San Francisco: ASP), 110  
 Mason, B. D., Wycoff, G. L., Hartkopf, W. I., Douglass, G. G. & Worley, C. E. 2001, *AJ*, 122, 3466 (WDS)  
 Mason, B. D., Hartkopf, W. I., Wycoff, G. L., et al. 2004, *AJ*, 127, 539  
 Mason, B. D., Hartkopf, W. I., Raghavan, D., et al. 2011, *AJ*, 142, 176  
 Nordström, B., Mayor, M., Andersen, J., et al. 2004, *A&A*, 418, 989  
 Novakovic, B. & Todorovic, N. 2006, *Ser. AJ*, 172, 21  
 Pecaut, M. J. & Mamajek, E. E. 2013, *ApJS*, 208, 9  
 Ricker, G. R., Winn, J. N., Vanderspek, R., et al. 2014, in *Society of Photo-Optical Instrumentation Engineers (SPIE) Conference Series, Vol. 9143, Space Telescopes and Instrumentation 2014: Optical, Infrared, and Millimeter Wave*, 914320  
 Szentgyorgyi, A. H., & Fűrész, G. 2007, *Precision Radial Velocities for the Kepler Era*, in *The 3rd Mexico-Korea Conference on Astrophysics: Telescopes of the Future and San Pedro Mártir*, ed. S. Kurtz, *RMxAC*, 28, 129  
 Tokovinin, A. 2016, *ORBIT: IDL software for visual, spectroscopic, and combined orbits*. Zenodo, doi:10.2581/zenodo.61119  
 Tokovinin, A. 2018a, *ApJS*, 235, 6  
 Tokovinin, A. 2018b, *Inf. Circ.* 196, 1  
 Tokovinin, A., Latham, D. W., & Mason, B. D. 2015, *AJ*, 149, 195  
 Tokovinin, A. & Latham, D. W. 2017, *ApJ*, 838, 54  
 Tokovinin, A., Mason, B. D., Mendez, R. A., et al. 2019, *AJ*, 158, 48  
 Tokovinin, A. A. & Smekhov, M. G. 2002, *A&A*, 383, 118  
 Zirm, H. & Rica, F. 2012, *Inf. Circ.* 177, 1